Supplementary Materials: Local Oxidation Nanolithography on Metallic Transition Metal Dichalcogenides Surfaces

Elena Pinilla-Cienfuegos, Samuel Mañas-Valero, Efrén Navarro-Moratalla, Sergio Tatay, Alicia Forment-Aliaga and Eugenio Coronado

S1. Crystal growth and characterization of TMDCs

(1) TaS_2

2H-TaS_2 crystals were synthesized from the elemental components in a two-step process by chemical vapor transport (CVT). Firstly, a polycrystalline sample was obtained by ceramic combination of stoichiometric ratios of the metal and chalcogen as described elsewhere [1]. Powder starting materials were intimately mixed, placed inside an evacuated quartz ampoule and reacted at 900 °C during 9 days. The resulting free-flowing glittery grey microcrystals were then transformed into large single-crystals by the CVT methodology. 1g of TaS_2 polycrystalline material together with 275 mg of I_2 were loaded into a 500 mm long quartz ampoule (OD: 18 mm, wall-thickness: 1.5 mm). The mixture was thoroughly stashed at one end of the ampoule and the latter was exhaustively evacuated and flame-sealed. The quartz tube was finally placed inside a three-zone split muffle where a gradient of 50 °C was established between the leftmost load (800 °C) and central growth (750 °C) zones. A gradient of 25 °C was also set between the rightmost and central regions. The temperature gradient was maintained constant during 15 days and the muffle was eventually switched off and left to cool down at ambient conditions. Millimetric TaS_2 crystals were recovered from the ampoule's central zone, exhaustively rinsed with diethyl ether and stored under a N_2 atmosphere.

Phase purity was confirmed by fitting the XRPD pattern (Figure S1.1). The fit yield to a single crystallographic phase with $a = b = 3.315$ (1) Å, $c = 12.083$ (4) Å, $\alpha = \beta = 90°$, $\gamma = 120$ °, in accordance with the values reported in the literature [2].

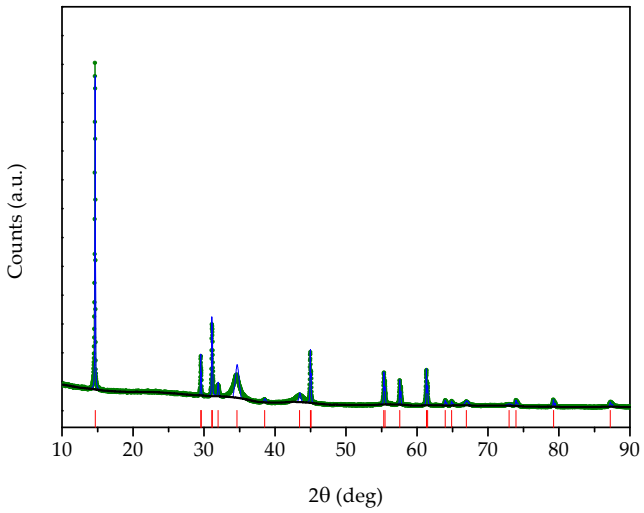

Figure S1.1. 2H-TaS_2 XRPD pattern (green) and unit cell refinement (blue). Peaks positions are marked with vertical red lines and the background with a black line.

(2) $TaSe_2$

1g of polycrystalline 2H-$TaSe_2$ was processed using the same CVT procedure and the same experimental conditions used for the growth of 2H-TaS_2. This resulted in the growth of very homogeneous samples of hexagonal flake-like crystals of 2H-$TaSe_2$. These crystals were recovered

from the growth zone of the ampoule and thoroughly rinsed with diethyl ether and then stored in a N_2 atmosphere.

Phase purity was confirmed by fitting the XRPD pattern (Figure S1.2) to a single crystallographic phase: $a = b = 3.4391$ (3) Å, $c = 12.707$ (2) Å, $\alpha = \beta = 90°$, $\gamma = 120°$, in accordance with the values reported in the literature [2].

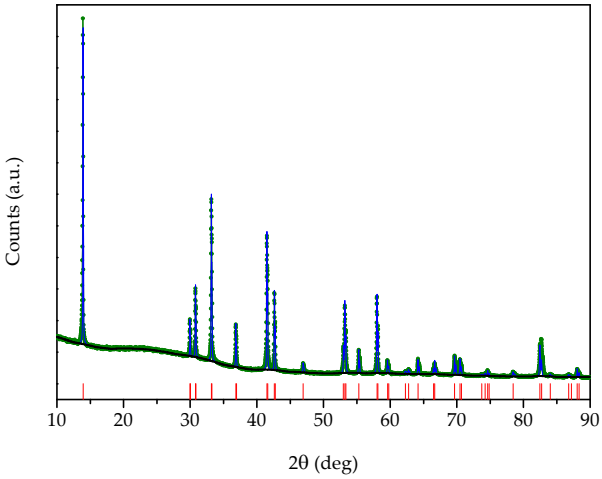

Figure S1.2. 2H-$TaSe_2$ XRPD pattern (green) and unit cell refinement (blue). Peaks positions are marked with vertical red lines and the background with a black line.

(3) NbS_2

1g of polycrystalline NbS_2 was processed using the same CVT procedure and the same experimental conditions used for the growth of 2H-TaS_2. After the CVT process, millimetre long hexagonal prisms could be observed in the growth zone of the fused silica vessel. Single-crystalline specimens of 2H-NbS_2 were thoroughly rinsed with diethyl and finally stored in a N_2 atmosphere.

Phase purity was checked by fitting the XRPD pattern (Figure S1.3). The fit yield to a single crystallographic phase with $a = b = 3.321$ (1) Å, $c = 11.945$ (5) Å, $\alpha = \beta = 90°$, $\gamma = 120$, in accordance with the values reported in the literature [2].

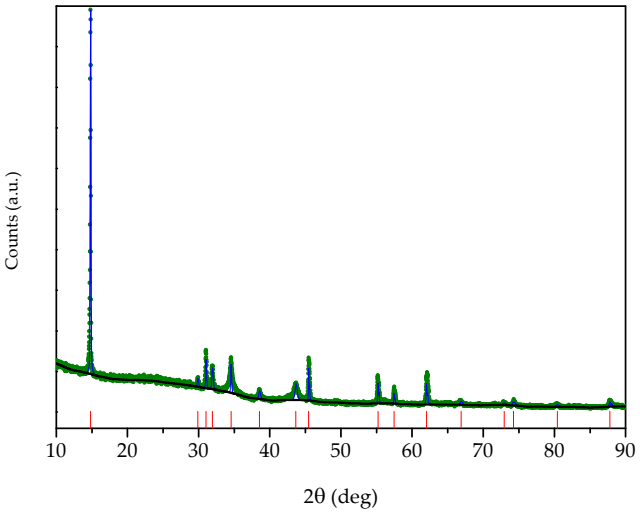

Figure S1.3. 2H-NbS_2 XRPD pattern (green) and unit cell refinement (blue). Inset: Photography of a 2H-NbS_2 crystal. Peaks positions are marked with vertical red lines and the background with a black line.

During the exfoliation of NbS_2 crystals, several needles were observed next to the platelet like flakes (characteristic of the 2H phase). The study of the Transition Electron Microscopy (TEM) images and EDX analysis on one single needle (Figure S1.4) gives rise to the following atomic composition (%): S 67.7 and Nb 32.3, in good accordance with the expected one for NbS_2. The Fast Fourier Transform (FFT) image indicates a rhombohedral structure. Thus, needles can be assessed as the 3R polytype of NbS_2.

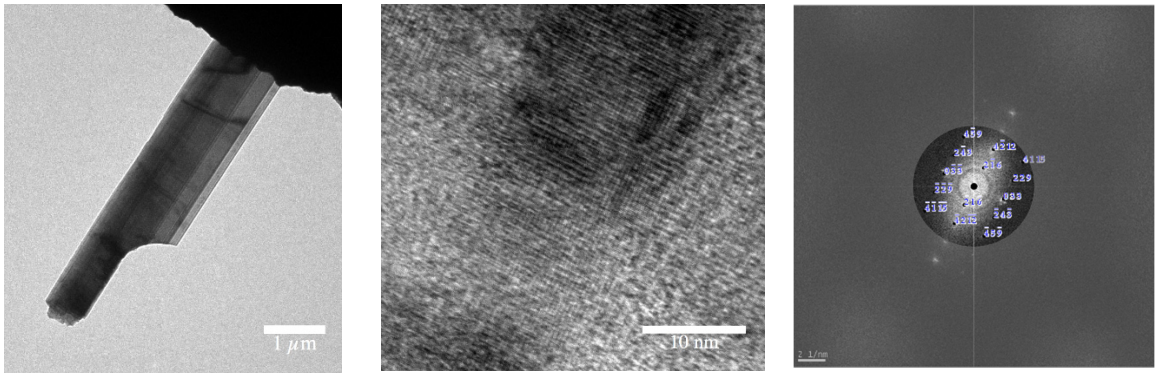

(**a**) (**b**) (**c**)

Figure S1.4. TEM characterization of 3R-NbS_2 needles. (**a**) TEM image of the inspected needle; (**b**) detail with atomic scale area; and (**c**) TEM FFT diffraction pattern of (**b**).

(4) $NbSe_2$

In an analogous way as described for the crystal growth of 2H-TaS_2, 1g of polycrystalline $NbSe_2$ was processed using the same CVT procedure. As a result, homogeneous hexagonal-like crystals of 2H-$NbSe_2$ with a high aspect ratio and several millimetres in length appeared in the growth zone. Crystals of 2H-$NbSe_2$ were thoroughly rinsed with diethyl ether before storing in a N_2 atmosphere.

Phase purity was confirmed by fitting the XRPD pattern (Figure S1.5). The fit yield to a single crystallographic phase with $a = b = 3.4460$ (4) Å, $c = 12.549$ (2) Å, $\alpha = \beta = 90°$, $\gamma = 120$, in accordance with the values reported in the literature [2].

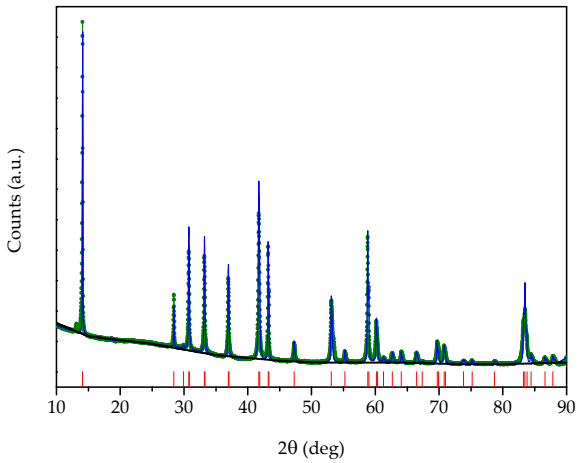

Figure S1.5. 2H-NbSe2 XRPD pattern (green) and unit cell refinement (blue). Peaks positions are marked with vertical red lines and the background with a black line.

S2. Schematic figure of Dynamic-tip LON vs. Static-tip LON

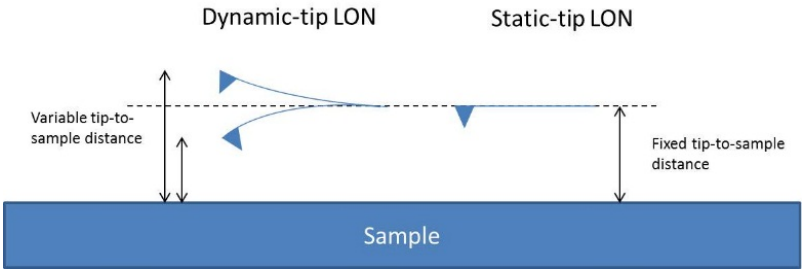

Figure S2. Sketch describing AFM tip movement during dynamic-tip LON and static-tip LON processes.

S3. Etching in thin flakes

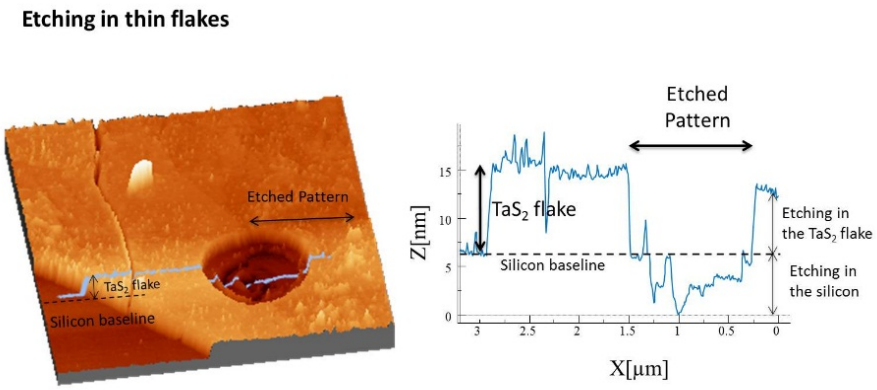

Figure S3. Etching on a thin TaS2 layer. 3D topography image of an HF etched oxide dot (left) and the corresponding height profile (right).

S4. LON on $NbSe_2$

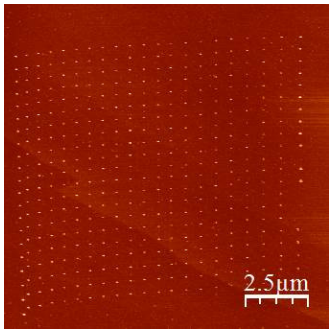

Figure S4. AFM topography image of a matrix of 20 × 20 oxide dots onto the $NbSe_2$ surface by static-tip LON. Image size: 12.5 μm × 12.5 μm.

References

1. Gamble, F.; DiSalvo, F.; Klemm, R.A.; Geballe, T. Superconductivity in layered structure organometallic crystals. *Science* **1970**, *168*, 568–570.
2. Wilson, J.A.; Yoffe, A.D. The transition metal dichalcogenides discussion and interpretation of the observed optical, electrical and structural properties. *Adv. Phys.* **1969**, *18*, 193–335.